Available online at www.sciencedirect.com
ScienceDirect
Physica A 380 (2007) 98–108
PHYSICA A
www.elsevier.com/locate/physa

Investigation of global solar magnetic field by computational topology methods

N.G. Makarenko[a], L.M. Karimova[b], M.M. Novak[c,*]

[a]*Pulkovo Astronomical Observatory, 65/1, Pulkovo Highway, 196140, St.Petersburg, Russia*
[b]*Institute of Mathematics, 125 Pushkin Street, 050010, Almaty, Kazakhstan*
[c]*Faculty of CISM, Kingston University, Surrey KT1 2EE UK*

Received 2 November 2006; received in revised form 14 February 2007
Available online 28 February 2007

Abstract

This paper analyzes the dynamics of large scale or background solar magnetic field by the methods of computational topology. First of all, we investigate global reversal of the field. A reversal refers to a change in the sign of the field dipole component on the solar poles. The synoptic chart is a synthetic representation of solar structures visible during one rotation of the Sun. A time sequence of synoptic charts, representing the distribution of a sign of background magnetic field averaged over one 27-days-long Carrington rotation, is used here. The rate of change of a number of ε disconnected components on the charts, formed by unipolar magnetic structures, versus resolution is characterized by the disconnectedness index. The value of this index may coincide with the box dimension of simple fractals. We have established a different behavior of ε disconnected components for magnetic structures with and without reversals. Reversals are characterized by the disappearance of distinguishing scales of magnetic structures (fractality) and, as a result, by larger scaling interval for estimation of the disconnectedness index. The obtained results may be interpreted as demonstrating a self-organizing criticality in large scale magnetic field dynamics. Moreover, we apply homology theory to estimate 'spottiness' of synoptic charts by means of the Betti number β_1. It characterizes number of 'holes' formed as inclusions into unipolar regions of the magnetic field of opposite sign. It appears that time series of the Betti number as well as index of disconnectedness have two modes, particularly, quasi-biennial oscillation and 11-year oscillations.

Keywords: Solar magnetic field reversal; Synoptic charts; Disconnectedness index; Betti numbers

1. Introduction

Dynamical regimes of an extended nonlinear system possess temporal and spatial complexity. The former is traced by means of time series of 'integral' parameters, which allows to consider the system as a point source of a signal. Contemporary methods of time series analysis and reconstruction of a topological model of

*Corresponding author.
E-mail addresses: ng-makar@mail.ru (N.G. Makarenko), karimova@math.kz (L.M. Karimova), novak@kingston.ac.uk (M.M. Novak).

0378-4371/$ - see front matter © 2007 Elsevier B.V. All rights reserved.
doi:10.1016/j.physa.2007.02.052

dynamical system from scalar data are adapted to such data [1,2]. The latter, the spatial complexity, is represented by observations of snapshot sequences available either as matrixes of digital images or as topographical charts. Direct extension of Takens algorithm to matrix sequences results in laborious computation [3,4]. However, one can apply mathematical morphology methods [5–7], which make it possible to extract geometrical and topological information from charts and images. Such an information can be generated in terms of scalar time series. For example, morphological, also known as the Minkowski functionals, quantitatively describe an area, boundary length and connectedness, or the Euler characteristic, of the excursion set of a pattern [8]. This approach was successfully applied in radioecology [6] and in analyzing large scale solar magnetic field [7,9].

Nevertheless, two patterns, characterized by the same geometry, may be topologically different [10,13]. For example, two fractals can have the same box dimension, but may have different porosity. In this case methods of computational topology [11–14] may supplement the morphological pattern description. Topological properties are more fundamental than metric ones, but are more difficult to determine computationally. In spite of this, in this paper we use the computational topology methods to analyze a large scale solar magnetic field dynamics.

The structure of the paper is as follows. Section 2 describes briefly a magnetic cycle of solar activity. In Section 3 we outline the computational topology method and disconnectedness index and give some results of this index estimation for synoptic charts. Then we move to algebraic topology [14–16], estimate the Betti number β_1 and provide a possible interpretation of the obtained results.

2. Magnetic cycle of solar activity

The best known manifestations of the solar magnetic activity are the solar spots [17], possessing strong magnetic field of up to 4000 G. Cyclic variation of a number of solar spots was discovered by amateur-astronomer Heinrich Schwabe in 1843. Then in 1849, Rudolf Wolf introduced a solar activity index as a relative number of solar spots representing linear combination of spots and their groups, i.e., Wolf's numbers. Average cycle duration is 11.1 years, but in fact the cycle changes vary from 8.5 to 14 years, obtained from the minima, and from 7.3 to 17 years for time intervals between the neighbouring maxima.

In addition to the 11-years periodicity, called the Wolf–Schwabe cycles, a varying location of spots during each cycle is observed. First spots appear at the beginning of the cycle on the so-called Royal latitudes—a belt between 40° north and 40° south. Then, during a cycle evolution, spots appear closer to the equator. This effect was determined by Spörer in 1867 and is now known as the Spörer law or butterfly diagram.

The next interesting characteristic of solar activity dynamics is the Hale law, describing polarity of spots in the groups. The spots in the groups form bipolar active regions. There are *preceding* spots, *p*-spots, and *following* spots, *f*-spots, that are evaluated in a following way. In northern hemisphere, during a cycle, *p*-spots have a polarity of the north pole and *f*-spots have the polarity of the south pole. At the same time, in the southern hemisphere *p*-spots have the polarity of the south pole and *f*-spots have the polarity of the north pole. Polarity of the spots of the groups changes for the next solar activity cycle and results in 22 years magnetic cycle or the Hale cycle. Thus, it is assumed, that polarity of the spots is driven by magnetic fields of the poles.

Large scale magnetic structures with space resolution $>5^\circ$ are called global or background field of the Sun [18,19]. Deterministic dynamics becomes apparent in evolution of unipolar areas during approximately 11 years. These isolated elements are in fact bipolar structures, with one of their polarities being the same as the polar background and the other appearing in the form of inclusions of different polarity—the islands. The magnitude of the large scale magnetic field elements is less than in sunspots ($\sim$10 G). However, the elements are present everywhere on the Sun's surface, even at the minimum of Wolf–Schwabe cycles, i.e., they represent a permanent component of solar magnetism. The sum of the active regions is no more than twice the flux of the quiet Sun [19]. Neutral magnetic lines separating these areas form so-called H_α synoptic magnetic charts Fig. 1. The name of the chart is associated with the traditional technique of identification of neutral lines by means of daily spectroheliograms in H_α line.

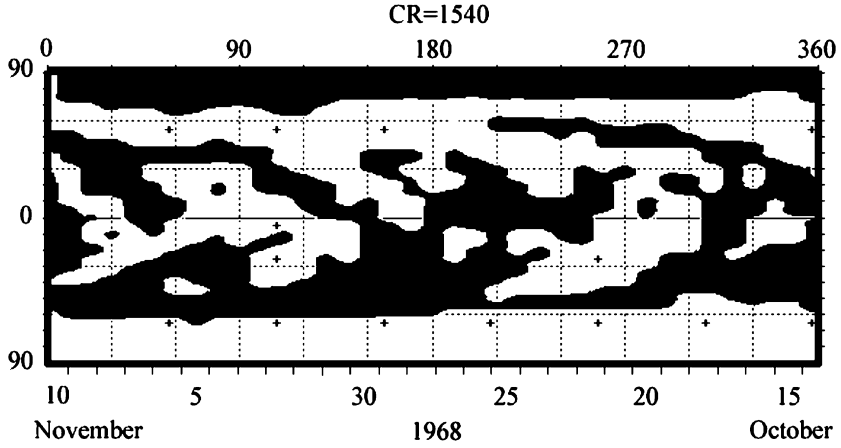

Fig. 1. Example of H_α chart for 1504 Carrington rotation (15 October–10 November 1968). Negative north polarity is shown by black color.

Thus the charts represent distribution of a sign of background magnetic field averaged over one 27-days-long Carrington rotation (CR)[1] in a form of cylindrical projection of Sun sphere. The sequence of synoptic charts covers years 1915–2002 [20,21]. Synoptic charts represent real structures at least homeomorphically except boundaries, so topological properties are normally preserved. Therefore, these charts are the most interesting for extracting geometrical and topological information about background field dynamics.

The polarity inversion of the global magnetic field is one of the most dramatic and mysterious effects of Sun activity. It does not occur synchronously in both hemispheres. There are cycles in which 2 or 3 reversals take place. The reversals may be accompanied by a situation, when both of the Sun's magnetic poles have the same sign. The process of polarity change can cover a few rotations of the Sun, so that there are synoptic charts, where north and south poles have magnetic field of the same polarity.

It is interesting that the magnetic field reversal is also known for the magnetic field of the Earth. This reversal can be traced in palaeomagnetic data [22], where changes of normal and reversed polarity over about 1 million years are observed up to the upper Cretaceous period. Moreover, long time intervals are known to exist when there were no polarity reversals and one such interval is within the Paleozoic period. It is likely that the Earth and solar inversions may have similar nature, associated with the existence of a strange attractor [23]. This is one of the reasons why analyzing the polarity reversals is of great interest.

3. Computational topology

3.1. Index of disconnectedness

A synoptic chart (Fig. 1) represents a finite set of compact elements called islands, which have a polarity opposite to that of the background. Thus, we consider a chart as a topological space. Let us recall [10,14] that a topological space X is connected if and only if it cannot be decomposed into the union of two nonempty, disjoint, closed sets. If such a decomposition exists then X is said to be disconnected—if there are two closed sets U and V such that $U \cap V = 0$ and $U \cup V = X$. The basic idea is to look at the set with a finite resolution ε and see how connectivity changes as we let $\varepsilon \to 0$. It is said that a subset X of metric space is ε *-disconnected* if it can be decomposed into sets that are separated by a distance of at least ε [10,12]. In other words, there are two closed subsets U and V such that $U \cup V = X$ and

$$d(U, V) = \inf_{x \in U, y \in V} d(x, y) > \varepsilon.$$

[1]A Carrington Rotation is a period of 27.2753 days, representing one full rotation of the Sun as seen from the Earth. The use of the numbers began on November 9, 1853.

Otherwise X is connected. So, the most interesting objects are ε-disconnected components of the set. The main question is what information about connectivity can be contained in disconnectedness as $\varepsilon \to 0$. We concentrate here on the main points, as details may be found elsewhere [11,12].

Let $C(\varepsilon)$ be the number of ε-components at a given resolution ε. The disconnectedness index γ is then

$$\gamma = \lim_{\varepsilon \to 0} \inf \frac{\log C(\varepsilon)}{\log(1/\varepsilon)}.$$

The index equals to a box-dimension for the simplest fractal sets, for example, for the middle-thirds Cantor set. However, in a more general case, the disconnectedness index distinguishes between sets with the same box-counting dimension.

In this paper we have estimated index of disconnectedness of synoptic charts. The question arises as to what is a difference of γ index behavior for unipolar magnetic structures without reversals in contrast to those with reversals.

One of the available methods [11,12] is based on a graph of the Minimal Spanning Tree (MST). The graph being free of cycles connects a discrete finite set of points in such a way that a sum of the edges is minimal. Sorting the lengths of MST branches makes it possible to carry out clusterizations of points by deleting branches with different length ε. However, it is difficult to adapt this method to topographic form of synoptic charts. Consequently, we used varying image resolution techniques of MatLab tools. Our approach analogous to the scale space method, which is used for image processing [24].

First of all, to test the algorithm we have estimated disconnectedness index γ of the Sierpinsky gasket, which was constructed by means of Iterated Function Systems (IFS). It is known [25,26] that a contraction is a map W from complete metric space (X, d) to itself provided that $d(W(x), W(y)) < d(x, y)$ for all $x, y \in X$. According to the Contraction Mapping Principle, W has a unique fixed point $W(x) = x$ in X. The distance $d(x, y)$ between the point $x \in X$ and a set $A \subset X$ in (X, d) is given by $d(x, A) = \inf_{y \in A} d(x, y)$. If $H = \{A_i\}$ is a set of compact subsets of X, then the Hausdorff metric h measures the distance between sets $A_i, A_j \subset H$ as $h(A_i, A_j) = \sup\{d(x, A_j), d(y, A_i) | x \in A_i, y \in A_j)\}$ and (H, h) is complete metric space. Introduction of $W(A_i) = \{W(x), \forall x \in A_i\}$ results in a set of contractive maps which are called IFS. Then the Hutchinson operator $\mathbf{W} : H \to H$ defined as $\mathbf{W}(A) = \cup_i W_i(A)$ is contraction in (H, h). The fundamental theorem of IFS [25] states that for any IFS there is a unique nonempty compact set $A \subset X$ (or a point in H) such that $A = \mathbf{W}(A)$. Moreover, for any $B \in H$ there is $\lim_{k \to \infty} \mathbf{W}^k(B) = A$, where $\mathbf{W}^k = \mathbf{W}(\mathbf{W}^{(k-1)})$ is the Hutchinson iteration operator. The invariant set A is the called an attractor of the IFS.

Deterministic algorithm for fractal construction [26] is based on computing a sequence of set $\{A_n = \mathbf{W}^n(A)\}$ starting from the initial set A_0. We construct the Sierpinski gasket on $A_0 = [0, 1] \times [0, 1]$ by IFS

$$W_1 \begin{bmatrix} x_1 \\ x_2 \end{bmatrix} = \begin{bmatrix} 1/2 & 0 \\ 0 & 1/2 \end{bmatrix} \begin{bmatrix} x_1 \\ x_2 \end{bmatrix} + \begin{bmatrix} 0 \\ 0 \end{bmatrix},$$

$$W_2 \begin{bmatrix} x_1 \\ x_2 \end{bmatrix} = \begin{bmatrix} 1/2 & 0 \\ 0 & 1/2 \end{bmatrix} \begin{bmatrix} x_1 \\ x_2 \end{bmatrix} + \begin{bmatrix} 0 \\ 1/2 \end{bmatrix},$$

$$W_3 \begin{bmatrix} x_1 \\ x_2 \end{bmatrix} = \begin{bmatrix} 1/2 & 0 \\ 0 & 1/2 \end{bmatrix} \begin{bmatrix} x_1 \\ x_2 \end{bmatrix} + \begin{bmatrix} 1/2 \\ 0 \end{bmatrix}.$$

Then attractor

$$A = \lim_{n \to \infty} \mathbf{W}^n(B), \quad B \in H$$

is called the Sierpinski gasket.

Random Iteration Algorithm allows construction of a multifractal gasket. In this case compressing map W_i is done according to a given probability $p_i, i = 1, 2, 3$, where $\sum_{i=1}^{3} p_i = 1$.

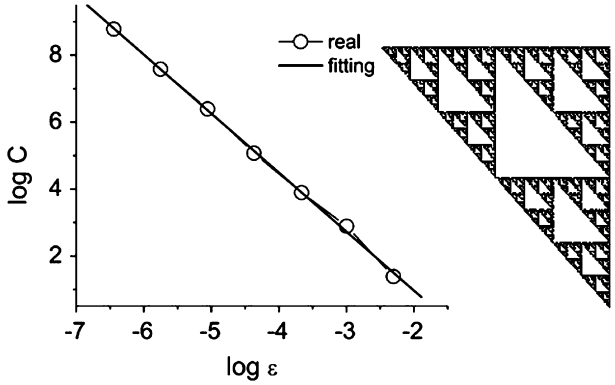

Fig. 2. Random Sierpinski gasket and log–log plot of ε-disconnected components $C(\varepsilon)$ for estimation index of disconnectedness γ.

Fig. 3. Example of changing image resolution for calculation of ε-disconnected regions $C(\varepsilon)$. The upper plot is initial tuple of charts; the lower one is example of tuples's resolution changing.

The value of γ index was estimated for such a gasket from the slope of the graph of $\log C(\varepsilon)$ versus $\log \varepsilon$ and equals 1.76 ± 0.03, compared to theoretical box dimension 1.58 (see Fig. 2), so algorithm gives acceptable precision.

To increase statistical significance of the calculation of ε-disconnected parts, $C(\varepsilon)$, a sequence of 10 synoptic charts was combined in one tuple, represented as an image in the upper panel of Fig. 3. The structure of the image changes with resolution, as one can see in Fig. 3 (lower panel), where the original image and the result of its modification are shown. This tuple does not contain any polarity reversal, as a northern (black) and a southern (white) regions have the corresponding homogeneous negative and positive magnetic fields around the poles, respectively.

At every change of an image resolution a number of ε-disconnected areas, $C(\varepsilon)$, was determined. Indices of disconnectedness, $\gamma_{(+)}$ and $\gamma_{(-)}$, for fields of positive and negative polarities, respectively, were estimated as a slope of dependence of the number of disconnected areas $C(\varepsilon)$ versus ε, from a log–log graph by the least-squares method.

The upper panel in Fig. 4 represents a tuple of charts from CR1400 to CR1409 with polarity reversals. A negative field at the north pole and a corresponding to it positive field at the south pole are replaced by positive fields at both poles. Such exchange takes place several times during these 10 solar rotations. The lower panel in Fig. 4 shows a plot which contains quite good scaling for both dependencies that correspond to $\gamma_{(+)} = 1.73 \pm 0.1$ and $\gamma_{(-)} = 1.73 \pm 0.04$. The value for the error in the disconnectedness index is obtained from the least-squares method.

The example without polarity reversals is shown in Fig. 5 for the fragment CR1210–CR1219. Comparison of Figs. 4 and 5 shows that, for the tuples with reversal behavior of $C(\varepsilon)$ versus ε, both polarities follow the power scaling and this extends over a large straight-line segment. Apparently, the reversals, especially those that happen repeatedly during some Sun rotations, form a 'fractal' field without fixed scales. The H_α-charts

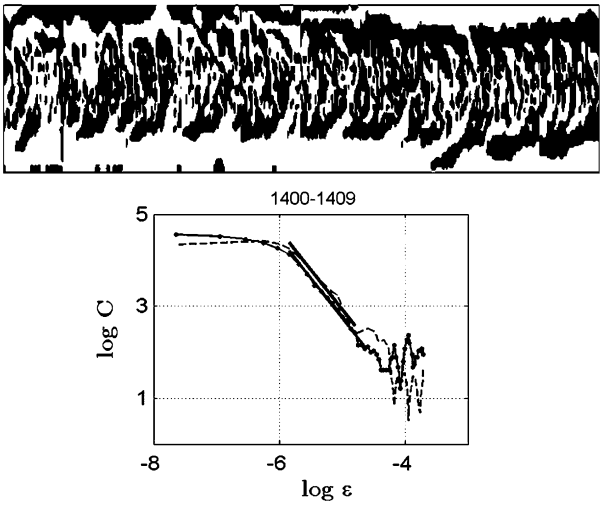

Fig. 4. A tuple which includes charts with polarity reversals for Sun rotations from CR1400 to CR1409 (top). These charts correspond to the maximum of 19th solar cycle. Disconnectedness indexes estimate is $\gamma_{(+)} = 1.73$ and $\gamma_{(-)} = 1.73$ for the fields of different polarity of this tuple (bottom). Dashed line corresponds to positive polarity of magnetic field, black line corresponds to negative one. The shown straight lines are regression lines to determine indexes $\gamma_{(+)}$ and $\gamma_{(-)}$.

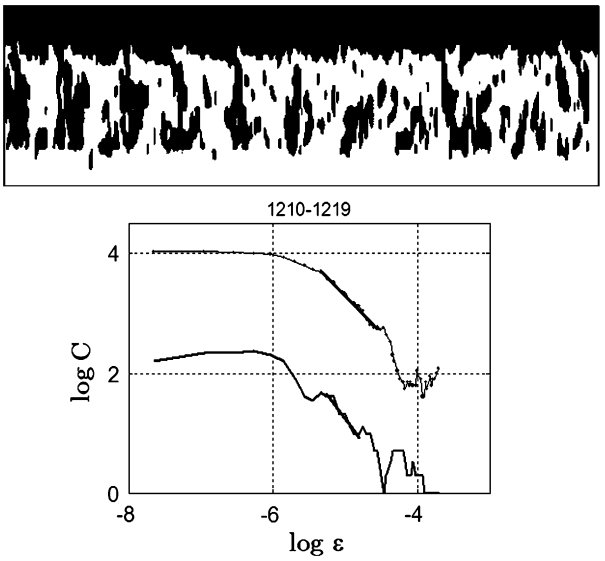

Fig. 5. A tuple which includes charts with constant polarities of poles for 1210–1219 rotations. The tuple is in the minimum between 17 and 18 solar cycles.

corresponding for these time intervals demonstrate a wide spectrum of different scale structures, both for a positive and a negative components of the field polarity.

For the tuples that do not contain any reversals (Fig. 5) on the magnetic field charts, some stable structure with separated scales appear. They lead to a partial disappearance of a power law in the distribution of numbers of ε-disconnected components. This effect appears, first of all, in the decrease of the scaling part and in greater error of an estimate of γ. The curves $\log C(\varepsilon)$ versus $\log \varepsilon$ for different polarity vary and that points out an unequal number of unipolar ε-disconnected components. This asymmetry perhaps is connected with known fact, that the north and south hemispheres do not play symmetric roles during a cycle [19]. To analyze the index of disconnectedness from one fragment to another, the values of $\gamma_{(+)}$ and $\gamma_{(-)}$ have been determined

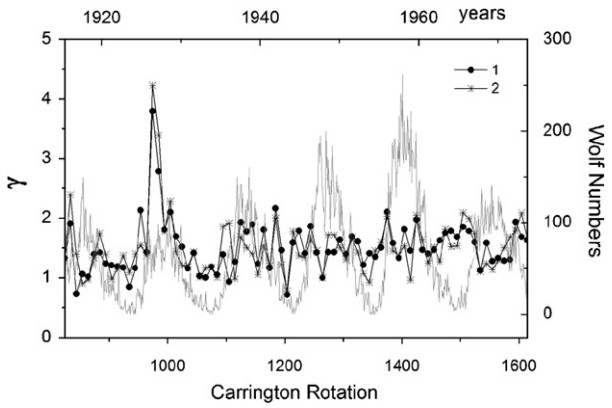

Fig. 6. Compare of indexes $\gamma_{(+)}$ and $\gamma_{(-)}$ behaviors (1 and 2 curves) with Wolf numbers variation.

for all available charts, in spite of computational difficulties (Fig. 6). Time series of disconnectedness index constructed for all available tuples demonstrate sharp fluctuations. Nevertheless, it is possible to see slight connection of indexes behaviours with the Wolf numbers variation.

Let us consider the obtained results. Is the reversal a phase transfer? A scaling accompanying the field inversions can be interpreted as 'obliterating' characteristic scales in magnetic structures. Roughly speaking, polarity reversals reflect the appearance of self-similar fractal field all over the Sun surface. On the other hand, a scale invariance in nonlinear systems is usually connected with a phenomenon of self-organized criticality [27]. This effect appears when an 'avalanche-like' growth of perturbation is observed in the dynamics of the process comprising more and more scales.

Situations similar to these appear during a phase transition of second type as well as in the bifurcation points of a dynamical system, when the type of its attractor changes under critical value of the control parameter. The property of these critical points is an ability of the small perturbations to have a considerable influence upon the whole system. Thus, a role of polarity reversals in large-scale field dynamics can be interpreted as the effect of self-organized criticality in magnetic dynamics of the field connected with a collapse of magnetic structures to a scaling of self-similar fractal.

3.2. Homology and the Betti numbers

To obtain complete description of topological complexity of synoptic charts, we apply the methods of computational topology related to a homology theory [13,15,16]. We begin with heuristic ideas. Any geometrical object can be separated into a combination of simple elements—topological cells or simplices. For example, let us cut one point from a circumference. Then we will get a combination of a point (or 0-simplex)[2] and an edge (or 1-simplex) with identified vertices. Now, let us remove from a torus T^2 one of its meridians that is circumference (Fig. 7). We get a cylinder from which we are removing a line—a torus parallel. The slit cylinder is a 'square' with pairwise identified edges. As a result we will obtain that a torus is a combination of one 0-simplex, two 1-simplices and one 2-simplex. We consider each simplex as a equivalence class of topologically similar elements. So all points of torus form class of 0-simpleces; meridians and parallels of torus form two different classes of 1-simplex, because it is not possible to transform one of them to another with a help of homeomorphisms. At last, a torus surface (a square) is a class of 2-simplex. We denote β_i as a number of torus equivalence classes with dimension i. Then an alternated sum

$$\chi(T^2) = \sum_{i=0}^{dim\, T^2} (-1)^i \beta_i$$

[2] k-simplex means simplex of dimension k.

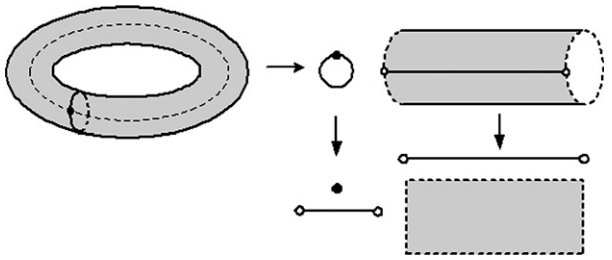

Fig. 7. Simplices of a torus. It is a combination of one 0-simplex, two 1-simplices and one 2-simplex.

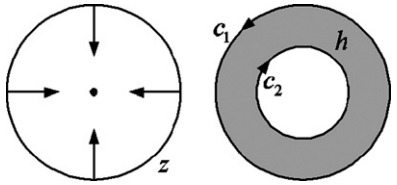

Fig. 8. Examples of cycles. The difference of two cycles $c_1 - c_2$ is a boundary of a ring area between them (right part). Cycle is homologous to zero: $z \sim 0$ (left part).

is called the Euler characteristic of torus T^2, and the numbers β_i are the ith Betti numbers. It is obvious, that for torus $\chi(T^2) = 1 - 2 + 1 = 0$.

Now we will give some formal definitions [14]. A k-simplex is the convex hull of $k+1$ affinely independent points. We use special names of the first few dimensions, *vertex* for 0-simplex, *edge* for 1-simplex and triangle for 2-simplex. We defined k-simplex as an order vertex set: $\sigma^k = [v_0, v_1, v_2, \ldots, v_k]$, where $\sigma^1 = [a, b]$ is an edge, $\sigma^2 = [a, b, c]$ is a triangle and so on. A linear combination of k-simplices $\sigma^i, dim\, \sigma^i = k$ is a k-chain: $c_k = \sum a_i \sigma^i, a_i \in Z$. Chains form an Abelian group C_k so that a sum of two k-chains $c'_k = \sum a_i \sigma^i, c''_k = \sum b_i \sigma^i, dim\, \sigma^i = k,\ a_i, b_j \in Z$ is $c'_k + c''_k = \sum (a_i + b_i)\sigma^i$. The boundary operator

$$\partial[v_0, \ldots, v_k] = \sum_{i=0}^{k} (-1)^i [v_0, \ldots, \hat{v}_i, \ldots, v_k],$$

where $\hat{v}_i$ indicated that $\hat{v}_i$ is deleted from the sequence, is defined as a homomorphism $C_k \to C_{k-1}$. An important property of this operator is $\partial\partial = \partial^2 = 0$. For example, $\partial[a, b, c] = \partial[b, c] - \partial[a, c] + \partial[a, b]$, i.e., a boundary of triangle is a directed 1-chain from the three edges: $\partial^2[a, b, c] = \partial[b, c] - \partial[a, c] - \partial[a, b] = c - b - (c - a) + b - a = 0$. The chains $c_k = 0$ are called cycles if $\partial c_k = 0$. They are a subgroup $Z_k = ker\, \partial_k \subset C_k$. Cycles contain their subgroup of boundaries $B_k = im\, \partial_{k+1} \subset Z_k$. Its elements are chains $c_k = \partial c_{k+1}$. Thus $B_k \subseteq Z_k \subseteq C_k$.

A contour c in the plane is a cycle. A cycle bounding some area lying completely in R^2 is a boundary. Any boundary is a cycle, but a cycle surrounding 'a hole' in a plane bounds nothing, i.e., is not a boundary. A sum of two cycles $c_1 + c_2$ is a cycle; a difference of two cycles $c_1 - c_2$ is a boundary of a ring area between them (see Fig. 8, right part). Any two cycles are homologous $c_1 \sim c_2$ if their difference is a boundary $c_1 = c_2 + \partial c_{k+1}$. A cycle which can be 'subtended' into a point (Fig. 8, left) is homologous to 0: $c \sim 0$.

This approach allows partitioning subgroup of cycles $Z_k \subset C_k$ on additional classes equivalent to boundaries B_k. These classes are named factor group of kth homologies $H_k = Z_k / B_k = ker\, \partial_k / im\, \partial_{k+1}$. A rank of free part H_k is the kth Betti number, $rank\, H_k = \beta_k$. Homology groups are finitely generated Abelian and in n-dimensional simplicial space has at most $n+1$ nontrivial homology groups. In R^2 the Betti numbers have intuitive meaning as follows: β_0 measures the number of connected components and β_1 counts the number of holes.

Previously we have already estimated one of the most useful topological invariants, Euler characteristic χ, for H_α synoptic magnetic charts [7,9]. But the Euler characteristic by itself is not powerful enough to

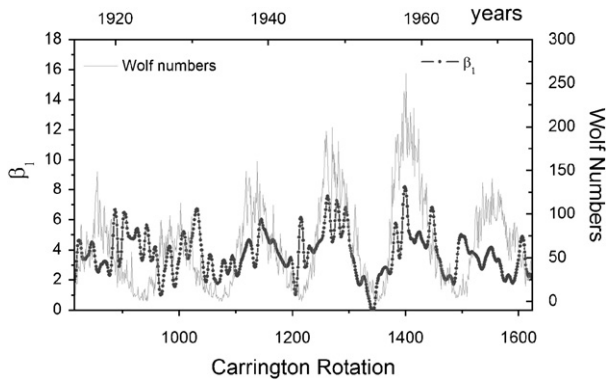

Fig. 9. Compare Wolf numbers W and β_1 after multifractal denoising time series for H_α synoptic magnetic charts.

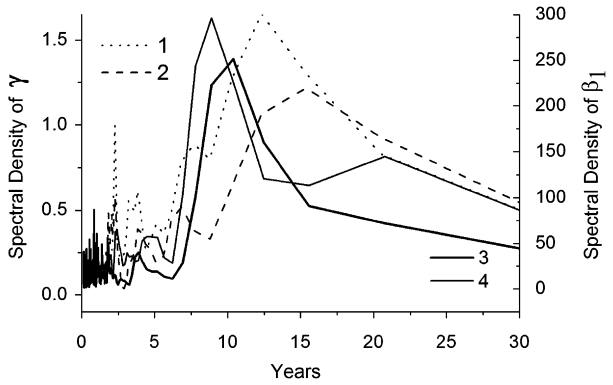

Fig. 10. Compare spectra of index of disconnectedness γ (1,2) and Betti numbers β_1 (3,4) time series. Lines 1 and 4 correspond to negative polarity of objects, 2 and 3 are spectra of positive polarity of magnetic field objects.

differentiate between surfaces [13]. Moreover, so far we know only a partial set of topological invariants [16], which means that even if all the known topological invariants of two topological spaces coincide, they may not be homeomorphic to each other. Rather, one can say that if two topological spaces have different topological invariants they are not homeomorphic to each other. Nowadays there are algorithms [14,16] and software, for example [28] to estimate Betti numbers in R^2 and R^3.

The Betti number β_1 has been computed for CR815–CR1629 H_α synoptic magnetic charts. The value β_1 is roughly estimated as a number of holes of synoptic charts or a number of cycles bounding areas of the same polarity located inside a region of another polarity. It characterizes a spottiness of H_α magnetic charts. Time series of β_1, after multifractal denoising [29] with the help of FracLab,[3] together with the Wolf numbers are shown in Fig. 9. The variations of β_1 time series and the Wolf numbers W are similar (cf. Fig. 9) except for short intervals.

Fig. 10 shows spectral density plots obtained with the help of the Hamming window for time series of β_1 by means of 3 and 4 curves and index of disconnectedness γ by curves 1 and 2. All four time series demonstrate quasi-biennial oscillation and 11-year mode. It is interesting that only β_1 time series for negative polarity has produced feebly marked 22-years mode (see curve 4 in Fig. 10). We have no explanation of this result, but the same mode appeared for the Euler characteristics χ from the same synoptic charts earlier [7].

[3]http://www.irccyn.ec-nantas.fr/hebergement/FracLab.

4. Conclusion

Within the frame of computational topology we have estimated, in this paper, the disconnectedness index and the Betti number β_1 for CR815–CR1629 synoptic magnetic charts. This interval covers approximately 60 years or five solar cycles.

Index of disconnectedness estimates the scale features of magnetic structures of the Sun depending on the resolution. The Betti numbers are necessary for full description of topological structures as they differentiate between structures with similar geometry, but with different number of holes.

On the basis of obtained results, magnetic field reversal can be interpreted as the product of self-organized criticality, so the reversal might be regarded as a particular form of phase transition. The reversals result in the disappearance of preferential scales in magnetic structures of the Sun. After a reversal, magnetic structures of particular scales reappear.

Estimation of the Betti number, β_1, of synoptic charts has demonstrated, that topology of global magnetic field is characterized mainly by two basic periods: quasi-biennial oscillation and 11- year oscillations. These modes exist also for index of disconnectedness γ. Moreover, correlation dimension $\nu = 2.3$ of a phase reconstruction of the β_1 time series means that dynamics allows models with two or three degrees of freedom (modes), that conforms with the recent analysis of the topological dynamics of the sunspot cycles [30]. As long as, background field apparently is a driver of solar activity, our result is in support of a dual-mode model of dynamo [25,31].

All our experiments confirm that methods of computational topology can reveal an interesting information from H_α synoptic magnetic charts. We assert that the knowledge of topologically persistent [13] characteristics will allow us to refine the type of a model suitable for the description of complex solar magnetic dynamics.

References

[1] Y.-C. Lai, N. Ye, Int. J. Bifur. Chaos 13 (2003) 1383.
[2] T. Sauer, J.A. Yorke, M. Casdagli, J. Stat. Phys. 65 (1991) 579.
[3] M. Rabinovich, A. Fabricant, L. Tsimring, Usp. Fiz. Nauk. 42 (1992) 1 (in Russian).
[4] U. Parlitz, Ch. Merkwirth, Phys. Rev. Lett. 84 (2000) 1890.
[5] K. Michielsen, H. De Raedt, Phys. Rep. 347 (2001) 461.
[6] N. Makarenko, L. Karimova, A. Terekhov, M.M. Novak, Physica A. 289 (2001) 278.
[7] N.G. Makarenko, L.M. Karimova, M.M. Novak, in: M.M. Novak (Ed.), Emergent Nature. Patterns, Growth and Scaling in the Sciences, World Scientific, Singapore, 2001, p. 197.
[8] R.J. Adler, The Geometry of Random Feilds, Wiley, New York, 1981.
[9] A.V. Mordvinov, I.I. Salakhutdinova, L.A. Plyusnina, N.G. Makarenko, L.M. Karimova, Solar Phys. 211 (2002) 241.
[10] V. Robins, Computational topology at multiple resolutions, Ph.D. Thesis, 2000. ⟨http://wwwrsphysse.anu.edu.au/∼vbr110/thesis/thesis.php⟩.
[11] V. Robins, J.D. Meiss, E. Bradley, Physica D 139 (2000) 276.
[12] V. Robins, J.D. Meiss, E. Bradley, Nonlinearity. 11 (1998) 913.
[13] V. Robins, Lecture Notes in Physics, vol. 600, 2002, p. 261.
[14] A. Zomorodian, Topology for Computing, Cambridge Monographs on Applied and Computational Mathematics, 2005.
[15] M. Gamaeiro, W.D. Kalies, K. Mischaikow, Phys. Rev. E 70 (2004) 035203(R).
[16] T. Kaczynski, K. Mischaikow, M. Mrozek, Computing Homology, Applied Mathematical Science, vol. 157, Springer, New York, 2004.
[17] H. Zirin, Astrophysics of the Sun, Cambridge University Press, Cambridge, MA, 1988.
[18] M.D. Altschuler, D.E. Troffer, G. Newkirk, Solar Phys. 39 (1974) 3.
[19] Z. Mouradian, I. Soru-Escaut, Astron. Astrophys. 251 (1991) 649.
[20] P.S. McIntosh, Annotated atlas of synoptic charts for solar cycle 20 (1964–1974). Carrington solar rotations 1484–1616. Boulder, 1979.
[21] V.I. Makarov, K.P. Sivaraman, Materilas of the world center data, Moscow, 1984 (in Russian).
[22] W.D. Parkinson, Introduction to Geomagnetism, Scottish Academic Press, Edinburg, 1983.
[23] Ya.B. Zeldovich, A.A. Ruzmaikin, D.D. Sokoloff, Magnetic Fields in Astrophysics, Gordon and Breach, New York, 1983.
[24] L.J. Florack, A. Kuijper, J. Math. Imagin Vision 12 (2000) 65.
[25] K. Falconer, Fractal geometry, Mathematical Foundations and Applications, Wiley, New York, 1990.
[26] M. Barnsly, Fractals Everywhere, Academic Press, Orlando, 1988.

[27] P. Bak, C. Tang, K. Wiesenfeld, Phys. Rev. A. 38 (1) (1988) 364.
[28] CHomP, ⟨http://www.math.gatech.edu/~chomp/software/⟩.
[29] J. Lèvy Vèhel, IMA Volumes in Mathematics and its Applications, vol. 132, 2002, p. 197.
[30] C. Letellier, L.A. Aguirre, J. Maquet, R. Gilmore, Astron. Astrophys. 449 (2006) 379.
[31] E. Benevolenskaya, Astrophys. J. 509 (1998) L49.